Inorganic Chemistry

Article

pubs.acs.org/IC

Water Oxidation Catalyzed by the Tetranuclear Mn Complex $[Mn^{IV}_4O_5(terpy)_4(H_2O)_2](ClO_4)_6$

Yunlong Gao, Robert H. Crabtree, and Gary W. Brudvig*

Department of Chemistry, Yale University, New Haven, Connecticut 06520-8107, United States

Supporting Information

ABSTRACT: The tetranuclear manganese complex $[Mn^{IV}_4O_5(terpy)_4(H_2O)_2](ClO_4)_6$ (**1**; terpy = 2,2′:6′,2″-terpyridine) gives catalytic water oxidation in aqueous solution, as determined by electrochemistry and GC-MS. Complex **1** also exhibits catalytic water oxidation when adsorbed on kaolin clay, with Ce^{IV} as the primary oxidant. The redox intermediates of complex **1** adsorbed on kaolin clay upon addition of Ce^{IV} have been characterized by using diffuse reflectance UV/visible and EPR spectroscopy. One of the products in the reaction on kaolin clay is Mn^{III}, as determined by parallel-mode EPR spectroscopic studies. When **1** is oxidized in aqueous solution with Ce^{IV}, the reaction intermediates are unstable and decompose to form Mn^{II}, detected by EPR spectroscopy, and MnO_2. DFT calculations show that the oxygen in the mono-μ-oxo bridge, rather than Mn^{IV}, is oxidized after an electron is removed from the Mn(IV,IV,IV,IV) tetramer. On the basis of the calculations, the formation of O_2 is proposed to occur by reaction of water with an electrophilic manganese-bound oxyl radical species, $^{\bullet}O-Mn_2^{IV/IV}$, produced during the oxidation of the tetramer. This study demonstrates that $[Mn^{IV}_4O_5(terpy)_4(H_2O)_2](ClO_4)_6$ may be relevant for understanding the role of the Mn tetramer in photosystem II.

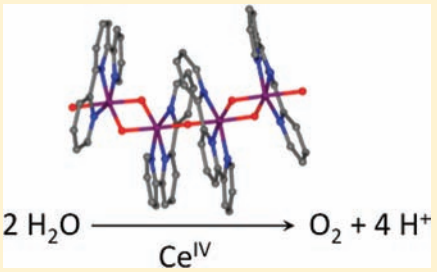

INTRODUCTION

The tetranuclear Mn cluster in the oxygen-evolving complex (OEC) of photosystem II (PSII) is the key catalyst for the oxidation of H_2O to O_2 in plants. The tetramer cycles through five distinct oxidation states or S states, S_0-S_4.[1] The most oxidized state, S_4, is unstable and returns to S_0 with release of O_2. However, despite intensive studies of the OEC, the detailed mechanism of water oxidation remains elusive, as well as the exact structure of the Mn tetramer as it cycles through the S states. X-ray absorption spectroscopic studies have provided evidence for the existence of Mn−(μ-O)$_2$−Mn and Mn−(μ-O)−Mn moieties in the Mn tetramer.[2] EPR/ENDOR studies[3,4] suggested that the four Mn ions of OEC are organized in a "3 + 1" fashion. The recent 1.9 Å X-ray crystal structure of PSII confirms these results and establishes the structure of the Mn ions in the OEC as a $CaMn_3O_4$ cubane linked to a fourth Mn.[5]

To mimic the natural active center, many high-valent multinuclear μ-oxo manganese complexes have been synthesized, and of these, high-valent manganese tetramers are of particular interest as structural models for the OEC.[6,7] The synthesized tetramers can be divided into six classes according to the atom connectivity of their Mn_4O_x core: (a) butterfly,[8−12] (b) square,[13] (c) adamantane,[14−16] (d) cubane,[17−22] (e) basket,[23] and (f) linear.[24−27] Our Mn terpy tetramer[26] $[Mn^{IV}_4O_5(terpy)_4(H_2O)_2]^{6+}$ (**1**; terpy = 2,2′:6′,2″-terpyridine), with a pair of Mn−bis(μ-oxo)−Mn units connected via a mono-μ-oxo bridge, has Mn−Mn distances similar to those observed in the OEC and is one of only a few examples of a high-valent oxomanganese tetramer with coordinated waters.[8,9,27,28] Such complexes are of particular interest, because water is the substrate of the OEC.

Although many manganese tetramers have been synthesized, none has been reported to catalyze water oxidation by electrochemical means or in homogeneous solution by using sacrificial one-electron chemical oxidants. Recently, Brimblecombe et al.[29] reported the photon-assisted electrochemical oxidation of water using a catalyst inspired by the Mn_4Ca active site of OEC, a tetranuclear Mn−oxo cluster ($[Mn_4O_4L_6]^+$, L = $(MeOPh)_2PO_2^-$). However, UV light absorption by the Mn tetramer is required to initiate O_2 production, which is not the case in the OEC, and recent results have shown that UV light induces the formation of catalytic manganese oxide nanoparticles from $[Mn_4O_4L_6]^+$.[30]

We now show that **1** can catalyze water oxidation electrochemically and chemically. Previous studies showed that the Mn-terpy dimer $[(terpy)_2Mn_2^{III/IV}O_2(H_2O)_2]^{3+}$ (**2**) can catalyze water oxidation in aqueous solution[31,32] and on kaolin clay[33,34] with various primary oxidants. On kaolin clay, the predominant O_2 evolution path occurs by a bimolecular reaction.[33,34] Prior work has shown that electrochemical oxidation of **2** induces its dimerization to form **1**.[35] It has also been found that **1** and **2** interconvert in a pH-dependent equilibrium, with **2** favored above pH 2.5 and **1** favored at lower pH.[26] Under the acidic and oxidizing conditions generated when Ce^{IV} is used as a primary oxidant for water-oxidation catalysis, as in the study of **2** on kaolin clay, two $[(terpy)_2Mn_2^{IV/IV}O_2(H_2O)_2]^{4+}$ units, produced by oxidation of **2**, can in principle combine to form the tetramer **1**. Therefore,

Received: October 10, 2011
Published: March 21, 2012

the predominant O_2 evolution path on kaolin clay may in fact arise from the tetramer **1**.

In the current study, the proposed tetramer formation is, indeed, detected by diffuse reflectance UV/visible spectroscopy when **2** is adsorbed on kaolin clay. Moreover, when **1** is adsorbed on kaolin clay, a redox cycle is observed upon oxidation by Ce^{IV}. One of the reaction intermediates is Mn^{III}, as determined by parallel-mode EPR studies. When **1** is oxidized in aqueous solution with Ce^{IV}, the reaction intermediates are unstable and decompose to form Mn^{II}, detected by EPR spectroscopy, and MnO_2. Density functional theory (DFT) calculations were carried out to study the catalytic reaction mechanism. According to the calculations, the oxygen in the mono-μ-oxo bridge is oxidized after an electron is removed from the Mn(IV,IV,IV,IV) tetramer, and a $^{\bullet}O-Mn_2^{IV/IV}$ oxyl radical species is formed, which oxidizes water. This study suggests that **1** may be a useful model for understanding the function of the Mn tetramer in the OEC.

EXPERIMENTAL SECTION

Chemicals. $[Mn^{IV}_4O_5(terpy)_4(H_2O)_2](ClO_4)_6$ (**1**) was synthesized according to ref 26, and $[(terpy)_2Mn_2^{III/IV}O_2(H_2O)_2](NO_3)_3$ was synthesized according to ref 31. Kaolin clay was purchased from Fisher Scientific. $Ce(NO_3)_4$ solution (1 N) was purchased from Alfa Aesar. Nitric acid was purchased from J. T. Baker. All solutions were prepared using Millipore water.

Electrochemistry. Linear scan voltammetry and cyclic voltammetry (CV) measurements were performed with a potentiostat (Model 273 potentiostat/galvanostat, EG&G Princeton Applied Research) in a conventional three-electrode system at room temperature. A basal-plane carbon electrode (surface area 9 mm^2) was used as the working electrode, a platinum wire as the auxiliary electrode, and a saturated calomel electrode (SCE) as the reference electrode. The electrolyte used in the experiments was KNO_3 (0.1 M). For bulk electrolysis experiments, the three electrodes were inserted in a homemade cell. The cell was sealed after adding a small magnetic stir bar to the reaction solution (5 mL, pH 1.50), and then the cell was put in a water bath to avoid heating by the magnetic stirrer. The headspace of the cell was 15 mL (not including the volumes of the three electrodes).

GC-MS. GC-MS experiments were carried out with a Hewlett-Packard 5890 Series II gas chromatography instrument connected to a Hewlett-Packard 5971A Mass Selective Detector using a capillary column from Alltech (phase, EC-5; length, 30 m; i.d., 0.25 mm; film thickness, 0.25 μm).

Optical Studies. Optical spectra were recorded with a Varian Cary-50 UV−visible spectrophotometer at room temperature. Diffuse reflectance UV−visible spectra were recorded with a Varian Cary 3E UV−visible spectrophotometer using a 1 cm path length cuvette. The suspension solutions were prepared for measurement by mixing 20 mg of kaolin clay with 3 mL of an aqueous solution of **1** or **2** in a test tube, and the mixture was then transferred to a cuvette. The mixtures were stirred with a glass rod before the measurement. A mixture of 20 mg of kaolin clay and 3 mL of water was used for background measurements.

EPR Studies. EPR spectra were collected on a Bruker Biospin/ELEXSYS E500 spectrometer equipped with a TE012 dual-mode cavity and an Oxford ESR-900 liquid helium cryostat. All spectra were collected at 4 K on frozen samples with the following settings: microwave power, 1 mW; modulation frequency, 100 kHz; modulation amplitude, 9.22 and 5 G for parallel-mode and perpendicular-mode EPR measurements, respectively.

O_2 Assay. Oxygen evolution from aqueous solutions of **1** in the presence of Ce^{IV} was measured at 298 K by an oxygen probe (Clark electrode) connected to a YSI 5300A oxygen monitor with digital readout and interfaced to a computer for data logging. The sample chamber was maintained at 25 °C with a circulating water bath. In a typical run, 6 mL of $Ce(NO_3)_4$ solution (1 N) was introduced into the sample chamber. After equilibration (~5−10 min), 100 μL of an aqueous solution of **1** (0.055 μmol) was injected into the $Ce(NO_3)_4$ solution.

DFT Calculations. The B3LYP functional included in the Gaussian 03 package[36] was used in the DFT calculations. Minimum energy configurations were obtained in broken symmetry (BS) states. A combination of basis sets was implemented in order to perform efficient, yet sufficiently accurate, calculations. The mixed basis set includes the LACVP basis set to account for a nonrelativistic description of electron−core potentials (ECP's) for Mn, 6-31G(d) for oxo-bridge oxygens, 6-31G for water oxygens and nitrogens, and 3-21G for carbons and hydrogens.

RESULTS AND DISCUSSION

As a solid, **1** forms red-black needles as previously reported,[26] but the aqueous solution is orange-red. This color of **1** in solution faded much more quickly at high pH than at low pH, indicating that **1** is unstable under more basic conditions. All the experiments carried out in this study were, therefore, performed at low pH to avoid the decomposition of **1** in solution.

Linear scan voltammetry was used to study the electrochemical behavior of **1**. Because **1** is unstable at higher pH, aqueous solutions of **1** were studied at pH values below 2.2 (after pH adjustment with nitric acid). The experiments were carried out as follows: first a voltammetric scan of a blank solution at a specific pH was recorded as the background. A minimal amount of solid **1** was then added to the solution (the concentration of **1** was determined by UV/visible spectroscopy), and the voltammetric scan was recorded again. A scan rate of 10 mV/s was used in all the experiments. Parts a and b of Figure 1 show the linear scan voltammetric scans for **1** at pH 2.18 and 1.26, respectively. The potentials for oxidation of **1** at both these pH values, obtained by comparison with the background, are the same within experimental error (ca. 1.22 V vs SCE), indicating that no proton is lost during the initial oxidation. The catalytic current increases continually from 1.22 to 1.6 V, and no turning point is found, demonstrating that **1** undergoes redox cycling during the electrochemical experiment. The catalytic current increases with an increase of pH, with a ca. 2-fold increase (at 1.6 V vs SCE) from pH 1.26 to pH 2.18 when the concentration of **1** is 57 μM, suggesting that there is a deprotonation step in the catalytic reaction. The catalytic current at pH 2.18 increases with an increase of the concentration of **1** from 57 μM to 95 μM; however, the catalytic current at a potential of 1.6 V (vs SCE) increases only 18% when the concentration increases 67%, probably because the catalytic reaction is limited by the proton acceptor.

CV measurements were also carried out. Figure 2a shows the CVs for **1** at pH 1.84 at a scan rate of 100 mV/s. No significant change is found after 15 scans, indicating that the catalyst is stable under these conditions. To determine whether the catalyst is MnO_2, which may be produced during the oxidation of **1**, CV measurements of $MnHPO_4$ were carried out; Mn(II) is known to electrodeposit as insoluble manganese oxides under oxidizing and acidic conditions.[37] The black trace in Figure 2b is the CV for 310 μM $MnHPO_4$ at pH 1.84. The oxidation peak at 1.25 V vs SCE is due to the oxidation of Mn^{II} to MnO_2, and the two reduction peaks at 0.96 and 0.80 V are due to the stepwise reduction of MnO_2 to MnOOH and then to Mn^{II}, respectively.[37] After addition of 50 mM Na_2HPO_4 to the solution, those peaks disappear (red trace in Figure 2b) because the formation of MnO_2 is suppressed in the presence of high concentrations of HPO_4^{2-}. The peaks associated with the

dx.doi.org/10.1021/ic2021897 | Inorg. Chem. 2012, 51, 4043−4050

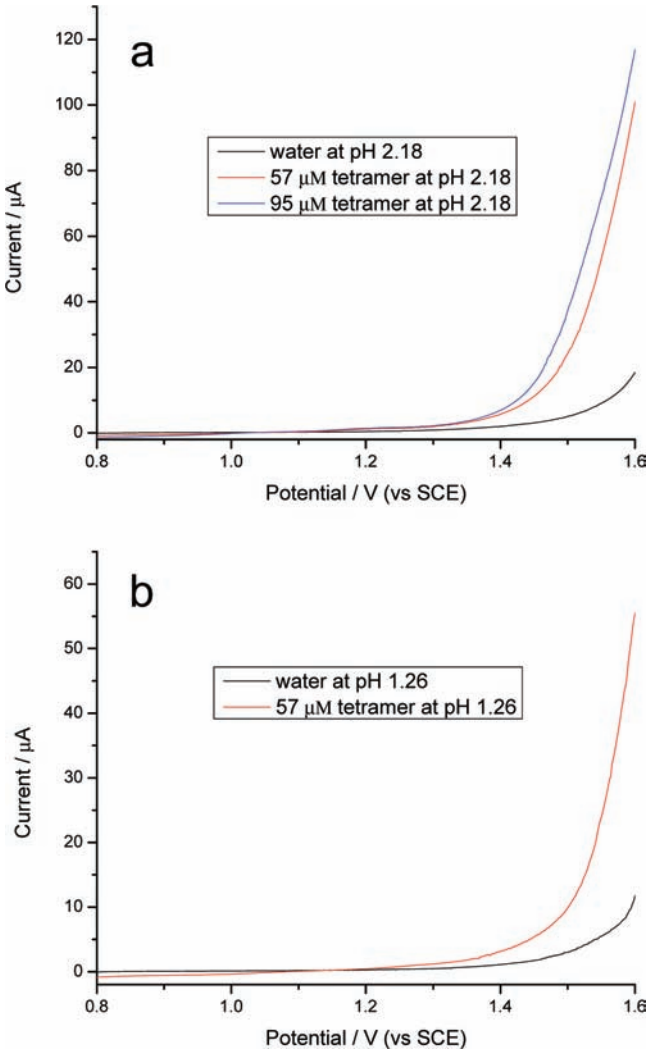

Figure 1. Linear scan voltammetry of **1** at pH 2.18 (a) and pH 1.26 (b).

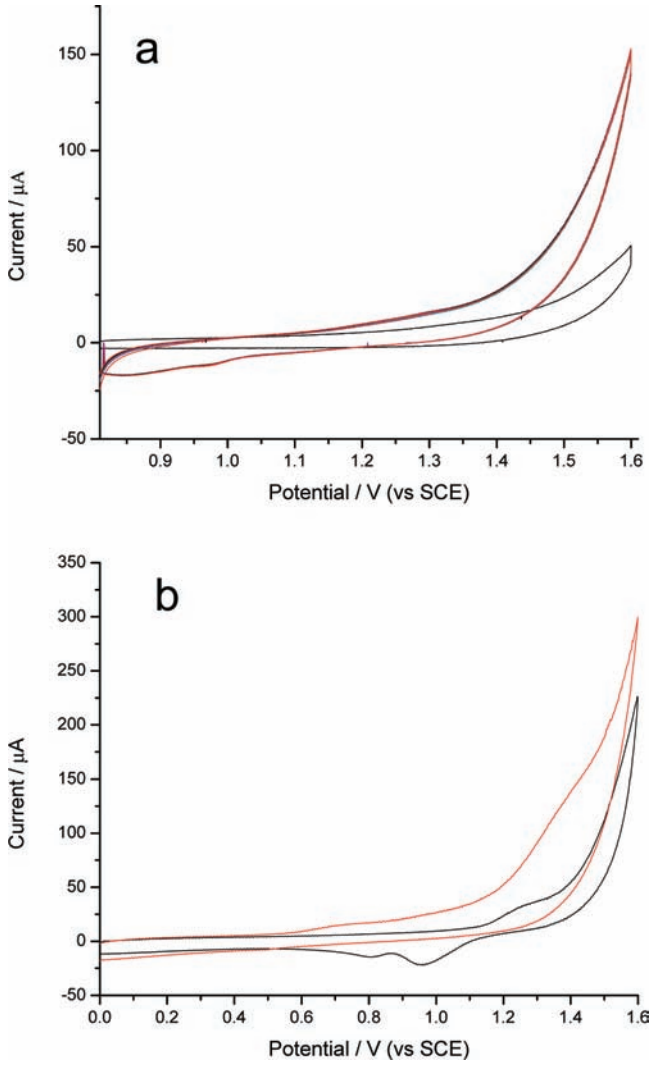

Figure 2. (a) CV of **1** (113 μM) at pH 1.84 (15 scans). The black trace is the background CV of water at pH 1.84. (b) CV of $MnHPO_4$ (310 μM) (black line) and of $MnHPO_4$ (310 μM) with addition of Na_2HPO_4 (50 mM) (red line). The scan rate is 100 mV/s for both cases.

reduction of MnO_2 are absent in the CVs for **1**, indicating that MnO_2 is not involved in the electrocatalytic reaction.

Bulk electrolysis of **1** (0.35 μmol) was performed at potentials of 1.4 and 1.6 V (vs SCE), respectively (Figure 3). The current was high at the beginning of the bulk electrolysis due to surface charging, and then the current decreased quickly. The number of coulombs passed vs time was recorded when the catalytic current became relatively stable. The number of coulombs passed increases almost linearly with time both for the solution of **1** and for the background solution. The difference in number of coulombs passed between the solution of **1** and the background at 1.4 V is much smaller than that at 1.6 V, consistent with linear scan experiments, which show that the catalytic current is much higher at 1.6 V than that at 1.4 V. The O_2 turnover number after a 1 h bulk electrolysis can be calculated from the number of electrons transferred. Although four electrons are needed for the oxidation of water to O_2, only one electron is needed per molecule of **1** for the first turnover, because **1** is a Mn(IV,IV,IV,IV) complex. Therefore, in the limit when the moles of electrons transferred is larger than the moles of **1** in solution, the formula for calculation of the turnover number (TN) is

$$TN = [m + (n - m)/4]/m$$

where n is the number of moles of electrons transferred due to the oxidation of **1** and m is the number of moles of **1** in the solution. The TN so calculated is 2.8 $\pm$ 0.5 (average of three experiments) at a potential of 1.6 V with 0.35 μmol **1**. The TN after a 1 h bulk electrolysis is small because the surface area of the working electrode is very small (9 mm^2).

GC-MS was also used to detect the O_2 produced after a one-hour bulk electrolysis by measurement of the ratio of the concentrations of O_2 to N_2 in the headspace of the cell. The relevant formula is

$$\Delta A = [(r_2 - r_1)]/r_0 \times A$$

where ΔA is the amount of O_2 produced due to oxidation of **1** (1.80 μmol), A is the amount of O_2 in the headspace of the cell before electrolysis, which is 145 μmol for 15 mL of headspace, r_0 is the ratio of O_2 to N_2 in the headspace of the cell before electrolysis, r_1 is the ratio of O_2 to N_2 in the headspace of the cell after electrolysis without **1** in solution, and r_2 is the ratio of O_2 to N_2 in the headspace of the cell after electrolysis with **1** in solution. The measured r_0, r_1, and r_2 values are 0.279 $\pm$ 0.003,

dx.doi.org/10.1021/ic2021897 | *Inorg. Chem.* 2012, 51, 4043–4050

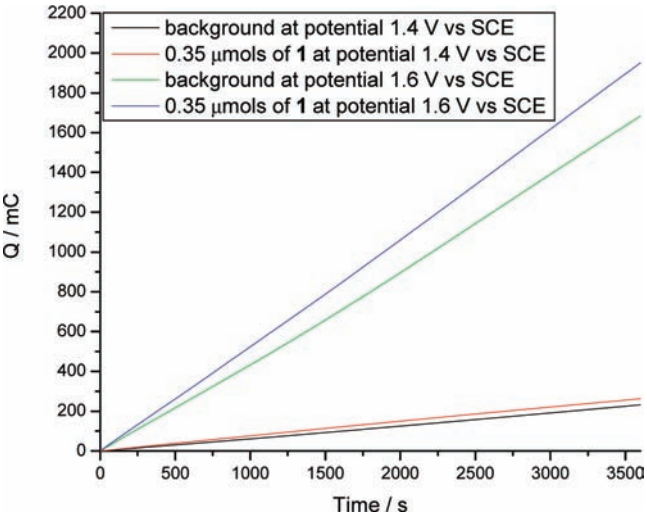

Figure 3. Coulombs passed (Q) vs time during the bulk electrolysis of 5 mL of a 0.35 μmol solution of **1** and background solutions at pH 1.50.

0.282 ± 0.004, and 0.293 ± 0.005, respectively (average of three experiments). The turnover number calculated in these GC-MS experiments is 3.18 ± 0.09, which agrees with the TN calculated from the number of electrons transferred due to the oxidation of **1**. Control experiments using 1 μmol of $MnSO_4$ or 1 μmol of the Mn(III,IV) bipyridine dimer[38] did not produce O_2.

Previous studies showed that the Mn terpy dimer **2** can catalyze water oxidation with various oxidants in aqueous solution[31,32] and on kaolin clay.[33,34] Because the oxidation of **2** in solution produces the Mn dimer of dimers complex **1**,[35] water oxidation may be catalyzed by **1** in the reactions. In this study, the behaviors of **1** and **2** on kaolin clay were examined by diffuse reflectance UV/visible spectroscopy. The purple color of **1** at pH 1.5 adsorbed on kaolin clay lasted 5 h in aqueous solution (pH 1.5). The purple color can last for up to 1 day if the sample is isolated by filtration and dried in air. Complex **1** is tightly associated with the clay and cannot be removed by washing, probably because of ion pairing with the anionic clay. The diffuse reflectance UV/visible spectrum of **1** on clay is shown in Figure 4a. The absorption peak at 483 nm is assigned to **1** adsorbed on clay. The slight red shift of the maximum absorption wavelength of **1** on kaolin clay compared to that in solution (red line in Figure 4a) is attributed to its adsorption on clay. Oxidation of the purple samples of **1** on kaolin clay by excess Ce^{IV} caused the purple color to disappear at once, but the color reappeared in seconds as the Ce^{IV} was consumed. The more Ce^{IV} added, the longer the time needed for the purple color to reappear. During the oxidation, a significant amount of tiny bubbles appeared on the clay, which can be attributed to O_2 formed by water oxidation catalyzed by **1**.

The diffuse reflectance UV/visible spectra of the oxidation of **1** on kaolin clay support the above observation. A fast scan from shorter wavelength (550 nm) immediately after addition of a drop of excess Ce^{IV} shows that λ_{max} changes significantly in the presence of Ce^{IV} (dotted line). The change of λ_{max} is due to the absorption of an intermediate produced during the reaction with Ce^{IV}, because the overall reaction is reversible. After 1 min when the Ce^{IV} has been consumed, the UV/visible spectrum is similar in both absorption maximum and intensity to that before the addition of Ce^{IV} (dashed line in Figure 4a). The

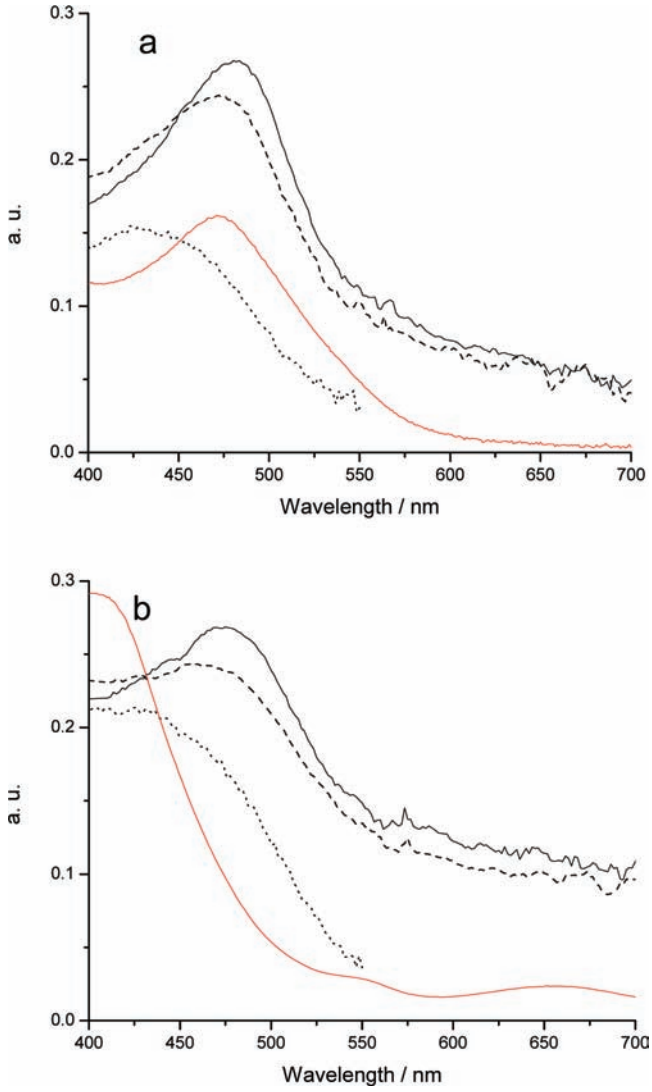

Figure 4. (a) Diffuse reflectance UV/visible spectrum of **1** on kaolin clay at pH 1.5 (solid black line) and fast scan (scan rate 3000 nm/min) after addition of 1 drop of excess Ce^{IV} (dotted line) and after 1 min (dashed line). The red line is the UV/visible spectrum of **1** in solution at pH 1.5. (b) Diffuse reflectance UV/visible spectrum of **2** on kaolin clay at pH 1.5 (solid black line) and fast scan (scan rate 3000 nm/min) after addition of 1 drop of excess Ce^{IV} (dotted line) and after 1 min (dashed line). The red line is the UV/visible spectrum of $[(terpy)_2Mn_2^{IV/IV}O_2(H_2O)_2]^{4+}$ in solution at pH 1.5. The background absorption of kaolin clay in water is subtracted in both cases.

slight blue shift of the absorption peak is due to the overlap of the absorption of Ce^{IV} and Ce^{III} at shorter wavelengths. The experiment was reproducible after the addition of another drop of excess Ce^{IV}. These experiments demonstrate that **1** on kaolin clay undergoes a redox cycle in the presence of Ce^{IV}. For comparison, the color of the adsorbed terpy dimer **2** is bluish purple when **2** is adsorbed on kaolin clay at pH 5. However, the color changed to purple with a maximum absorption wavelength that is similar to that of **1** on clay when the pH is adjusted to 1.5 (black solid line in Figure 4b), suggesting that the Mn dimer **2** also forms the tetrameric dimer of dimers **1** on clay. According to ref 33, **2** adsorbed on clay is autooxidized to form $(terpy)_2Mn_2^{IV/IV}O_2(H_2O)_2$ (the red line is the UV/visible spectrum of the $(terpy)_2Mn_2^{IV/IV}O_2(H_2O)_2$ dimer in solution) and two $(terpy)_2Mn_2^{IV/IV}O_2(H_2O)_2$ groups can combine to

dx.doi.org/10.1021/ic2021897 | Inorg. Chem. 2012, 51, 4043–4050

form the tetramer **1**.[35] The diffuse reflectance UV/visible spectrum (Figure 4b) during the oxidation of the purple species is similar to that of **1** on clay, suggesting that **1** is the species present under catalytic conditions. Previous studies showed that oxidation of **2** on kaolin clay can produce a significant amount of O_2, and the predominant path of O_2 evolution is via a bimolecular reaction of **2** adsorbed on kaolin clay.[33,34] According to the current study, the predominant O_2 evolution process is probably due to catalysis by the tetramer **1**, which is consistent with the proposed bimolecular reaction of **2** adsorbed on kaolin clay.

To study the reaction of **1** on kaolin clay with Ce^{IV}, the reaction products were examined by parallel-mode EPR spectroscopy. After Ce^{IV} was added to samples of either clay or clay with adsorbed **1**, the mixtures were immediately frozen at 77 K and then were transferred to the EPR cavity for the measurements. The parallel-mode EPR spectrum (Figure 5a) of the reaction product of **1** and Ce^{IV} on clay is very similar to the spectrum reported for a Mn^{III} species generated by photo-oxidation of Mn^{II} bound to Mn-depleted photosystem II.[39] Although parallel-mode EPR spectra are not very diagnostic of ligands, the signal observed in the reaction of **1** on kaolin clay with Ce^{IV} is likely from a mononuclear Mn^{III}-terpy species. No such Mn^{III} species was detected for a sample of clay and Ce^{IV} or clay with adsorbed **1**, indicating that a Mn^{III} species is a product of the reaction of **1** with Ce^{IV}. However, the Mn^{III} species was not detected when the reaction was carried out in solution (**1** was added to a Ce^{IV} solution and the mixture was immediately frozen at 77 K and then transferred to the EPR cavity for the measurement), probably because the Mn^{III} species is unstable in solution and can undergo disproportionation to form MnO_2 and Mn^{II}.[40] Figure 5b shows the perpendicular-mode EPR spectra of frozen solutions of **1** and Ce^{IV} (solid line) and $Ce(NO_3)_4$ (dashed line) at 4 K. The six-line signal around $g = 2$ indicates that Mn^{II} was produced after **1** was added to the Ce^{IV} solution.

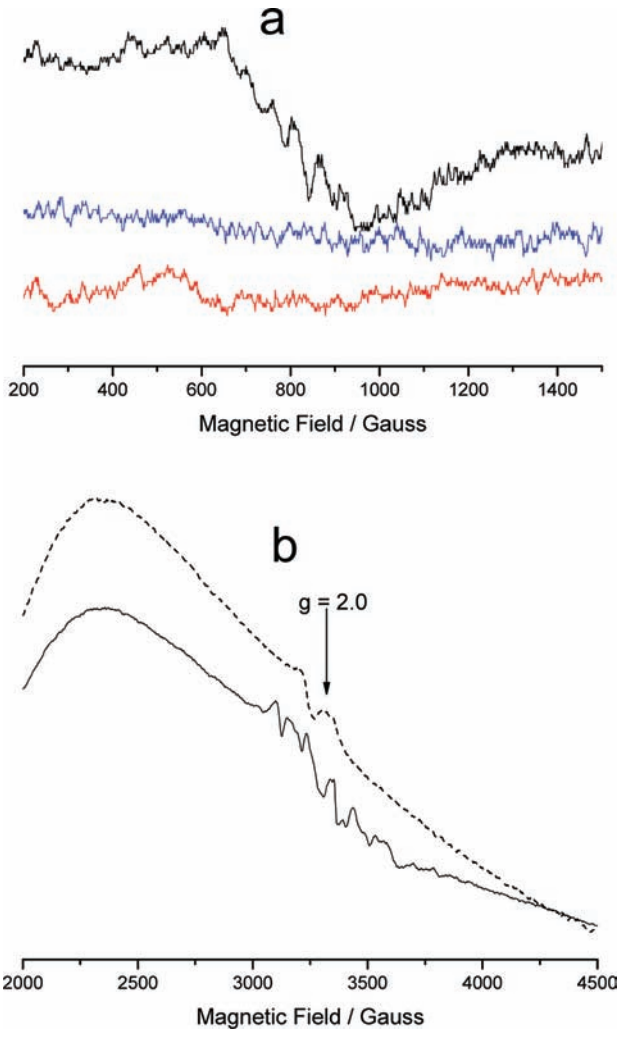

Figure 5. (a) 4 K parallel-mode EPR spectra of frozen samples of **1** on kaolin clay and Ce^{IV} (black line), kaolin clay and Ce^{IV} (red line), and kaolin clay with adsorbed **1** (blue line). (b) 4 K perpendicular-mode EPR spectra of frozen solutions of **1** and Ce^{IV} (solid line) and $Ce(NO_3)_4$ (dashed line).

The formation of MnO_2 was examined by UV/visible spectroscopy (Figure S1). After a small amount of **1** was added to a 10 mM $Ce(NO_3)_4$ solution (the concentration of **1** is 0.027 mM), the concentration of Ce^{IV} decreases significantly over 2 h, which is determined by the significant decrease of the absorbance at 400 nm. The absorbance of **1** at 477 nm also decreases somewhat, and the peak shape changes with a shoulder appearing at about 440 nm. Because the maximum absorption of MnO_2 is at about 440 nm,[41] the shoulder could be due to the absorption of MnO_2 nanoparticles produced in the reaction. The formation of MnO_2 is also confirmed by the observation of a brown precipitate after 6 h reaction of **1** (saturated concentration) and 1 N $Ce(NO_3)_4$ in solution.

Oxygen evolution from an aqueous solution of **1** in the presence of Ce^{IV} was measured at 298 K by an oxygen probe (Clark electrode). O_2 evolution was detected immediately after the injection of 0.055 μmol of **1** into 6 mL of 1 N $Ce(NO_3)_4$ solution (Figure S2), and the maximum concentration of O_2 was achieved in about 2 min. After that, the O_2 signal decreases almost linearly with time. The decrease of O_2 with time could indicate that an O_2-consuming reaction was being catalyzed after an initial O_2 evolution reaction. However, the formation of MnO_2 in the reaction of **1** and Ce^{IV} in solution could block the diffusion of O_2 through the channels of the membrane covering the Clark electrode and cause a decrease of the O_2 signal.

Prior work by Tagore et al.[42] shows O_2 evolution from a homogeneous aqueous solution of **2** in the presence of Ce^{IV}. Their data support water oxidation as the source of the evolved oxygen, and a high-valent multinuclear manganese species is required for oxygen evolution. However, the low pH conditions necessary for the use of Ce^{IV} prevent catalytic turnover due to the predominance of decomposition pathways. The key disadvantage of the use of Ce^{IV} as the primary oxidant is its inability to reoxidize low-valent mononuclear manganese species, generated during the oxygen-evolution reaction at low pH, to high-valent, oxo-bridged multinuclear manganese species. As a result, **2** cannot support a catalytic cycle at low pH. Our study of the reaction of **1** with Ce^{IV} in solution supports those conclusions.

To further understand the reaction mechanism, DFT calculations were performed. Figure 6 shows the structure of complex **1**, in the minimum energy configuration (total spin $S = 0$) obtained at the DFT/B3LYP level of theory. The analysis of Mulliken spin populations of Mn(1), Mn(2), Mn(3), and Mn(4) indicates spin populations of 2.773, −2.684, 2.677, and −2.782 au, respectively. This description corresponds to antiferromagnetic coupling of four high-spin Mn(IV) ions, each with $S = {}^3/_2$, giving a total spin of 0 for **1** in the ground

dx.doi.org/10.1021/ic2021897 | Inorg. Chem. 2012, 51, 4043−4050

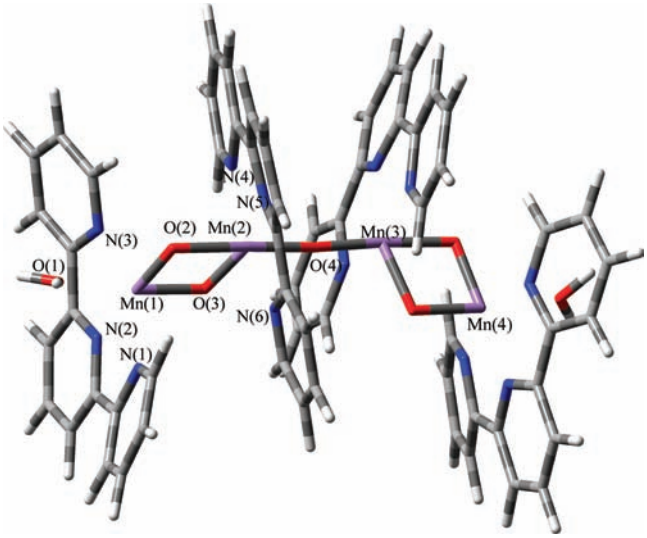

Figure 6. Structure of complex **1**, in the minimum energy configuration (total spin $S = 0$) obtained at the DFT/B3LYP level of theory.

state, in agreement with EPR data.[26] The bond lengths obtained by DFT calculations are very similar to those found in the experimental X-ray diffraction work (Table 1), suggesting

Table 1. Comparison of Selected Bond Lengths (Å) of 1 Obtained by DFT Calculations with Experimental X-ray Diffraction Data[26]

bond	X-ray structure	structure by DFT
Mn(1)−Mn(2)	2.764 29	2.784 31
Mn(1)−O(1)	2.018 00	2.022 09
Mn(1)−O(2)	1.754 35	1.748 62
Mn(1)−O(3)	1.787 64	1.784 89
Mn(2)−O(4)	1.769 03	1.788 65
Mn(1)−N(1)	1.990 12	2.044 21
Mn(1)−N(2)	2.022 27	2.013 61
Mn(1)−N(3)	2.029 48	2.049 23
Mn(2)−N(4)	2.034 41	2.035 36
Mn(2)−N(5)	1.986 29	2.009 99
Mn(2)−N(6)	2.036 03	2.033 69

that the DFT/B3LYP method and the basis sets used in the calculation are reasonable. The calculated charges of selected atoms of **1** are shown in Table 2. The charge at each Mn^{IV} is about 1.5, indicating that most of the charge of Mn^{IV} is delocalized over the ligands.

Because the electrochemistry experiments indicated that no proton is lost during the initial oxidation of **1**, the structure of complex **1** after the removal of one electron, in the minimum energy configuration (total spin $S = {}^1/_2$), was obtained at the

Table 2. Calculated Charge at Selected Atoms before and after Removal of an Electron from 1

atom	before	after
Mn(1)	1.491	1.520
Mn(2)	1.504	1.465
Mn(3)	1.512	1.472
Mn(4)	1.483	1.512
O(4)	−0.694	−0.369

DFT/B3LYP level of theory (Figure 7a). The analysis of Mulliken spin populations indicates antiferromagnetic cou-

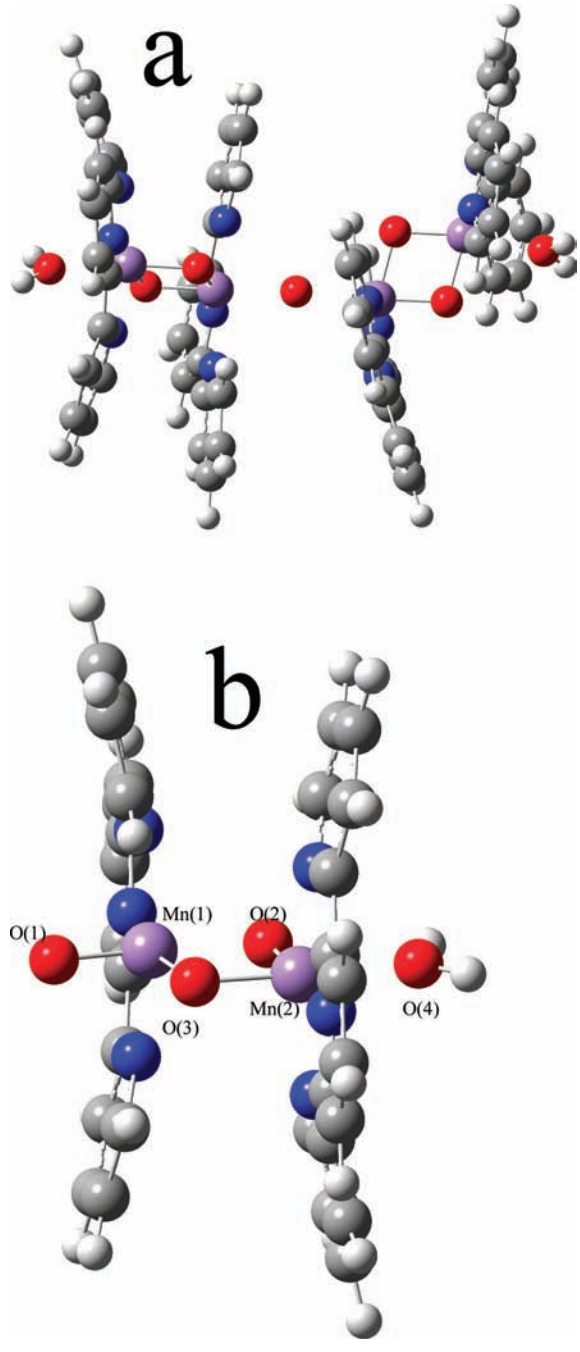

Figure 7. (a) Structure of complex **1** after the removal of one electron, in the minimum energy configuration (total spin $S = {}^1/_2$), obtained at the DFT/B3LYP level of theory. (b) Structure of the radical $^{\bullet}O-Mn_2^{IV/IV}$ species, in the minimum energy configuration (total spin $S = {}^5/_2$), obtained at the DFT/B3LYP level of theory.

plings between Mn(1) and Mn(2) and between Mn(3) and Mn(4) with spin populations of 2.884, −2.880, −2.872, and 2.898 au for Mn(1), Mn(2), Mn(3), and Mn(4), respectively, which corresponds to four high-spin Mn(IV) ions, each with $S = {}^3/_2$. Because the calculation indicates that all four Mn atms are Mn^{IV} after removal of one electron from **1**, the calculated oxidation is not metal centered. Rather, the calculated spin density for the oxygen in the mono-μ-oxo bridge is 0.9705,

dx.doi.org/10.1021/ic2021897 | Inorg. Chem. 2012, 51, 4043−4050

indicating that the bridging oxygen is oxidized. The calculated charge distribution (Table 2) shows that the charge at each Mn is about 1.5, which is similar to those before the electron removal, but the charge at the oxygen in the mono-μ-oxo bridge (−0.369) is much less negative than that before the electron removal (−0.668), confirming that the oxygen is oxidized. The Mn−O bond lengths (2.110 Å) for the mono μ-oxo bridge are much longer than those before the electron removal (1.789 Å), suggesting that those Mn−O bonds are easily broken after the electron removal.

On the basis of the DFT calculations, a sequence of reactions leading to formation of O_2 is proposed as shown in Scheme 1.

Scheme 1. Proposed Reaction Sequence for Catalysis of Oxygen Evolution by 1 on the Basis of DFT Calculations[a]

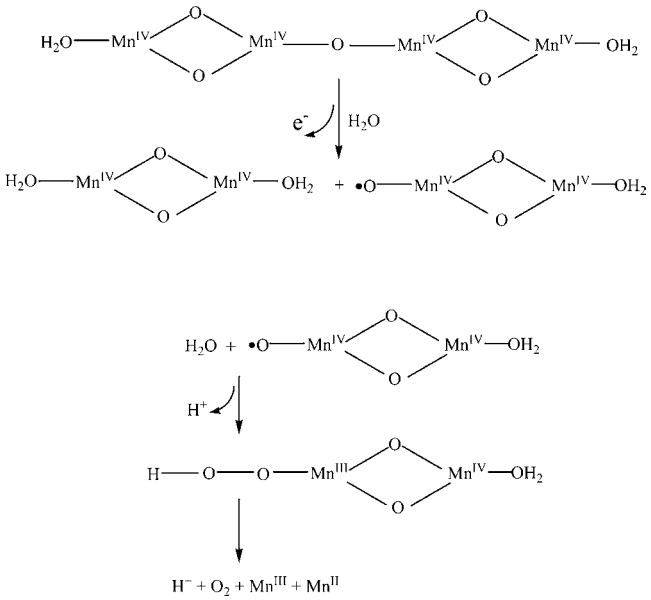

[a]terpy ligands are omitted for clarity.

After the removal of one electron from **1** in the presence of water, one $Mn_2^{IV/IV}$ dimer and one $^{\bullet}O-Mn_2^{IV/IV}$ oxyl radical species are formed. The $^{\bullet}O-Mn_2^{IV/IV}$ oxyl radical species is proposed to oxidize water to produce a peroxo intermediate that can then further react to produce O_2, Mn^{II}, and Mn^{III}. At an electrode surface, the peroxo intermediate is expected be rapidly oxidized to produce O_2 and the $Mn_2^{IV/IV}$ dimer. By combination of two $Mn_2^{IV/IV}$ dimers to form **1**, the initial catalyst would be regenerated. On kaolin clay, the peroxo intermediate may be stabilized so that further oxidation by Ce^{IV} could occur to generate O_2 and the $Mn_2^{IV/IV}$ dimer, followed by the combination of two $Mn_2^{IV/IV}$ dimers to re-form **1**.

DFT calculations were also performed on the $^{\bullet}O-Mn_2^{IV/IV}$ oxyl radical species. Figure 7b shows the structure of this species, in the minimum energy configuration (total spin $S = {}^5/_2$) obtained at the DFT/B3LYP level of theory. The calculated spin populations of O(1), Mn(1), and Mn(2) are −0.6512, 2.5900, and 2.7112, respectively, indicating antiferromagnetic coupling between O(1) and Mn(1). The Mn(1)−O(2) bond length (2.0318 Å) is longer than usual for a Mn−O single bond, presumably due to the unpaired electron on O(1). The calculated charge on O(1) (−0.291) is much less negative than for other oxygens (−0.607 (O2), −0.644 (O3), −0.742 (O4)), so that O(1) can access the oxygen of water and oxidize water to form a peroxo species.

This study supports a recent quantum mechanics/molecular mechanics (QM/MM) study of the catalytic cycle of water splitting in PSII, which suggests that water is oxidized by the electrophilic oxyl radical $Mn^{IV}-O^{\bullet}$ species formed in the S_4 state,[43] and recent work on other water-oxidation catalysts that invoke metal-oxyl species in water-oxidation catalysis.[44] Although the question of whether the fourth oxidation equivalent resides on a ligand (or on a Mn center) in the OEC is still strongly debated, our model compound study suggests that the μ-O ligand is more easily oxidized than Mn^{IV} in **1**.

CONCLUSIONS

The Mn-terpy tetramer $[Mn^{IV}{}_4O_5(terpy)_4(H_2O)_2](ClO_4)_6$ (**1**) can catalyze water oxidation at an electrode or on kaolin clay. However, the reaction intermediates in solution are unstable and decompose to produce Mn^{II} and MnO_2 when the reaction is carried out in aqueous solution with Ce^{IV} as the oxidant. DFT calculations suggest that O_2 is formed by reaction of water with an electrophilic manganese-bound oxyl radical species generated during the oxidation of the tetrameric Mn complex **1**. The tetranuclear complex **1** is a useful model for understanding the role of the $CaMn_4O_5$ cluster of the OEC in PSII, and a study of this model compound may contribute to understanding the reaction mechanism of the Mn tetramer in PSII.

ASSOCIATED CONTENT

Supporting Information

Figures giving UV/visible spectra and oxygen assay data. This material is available free of charge via the Internet at http://pubs.acs.org.

AUTHOR INFORMATION

Corresponding Author

*Tel: 203-432-5202. Fax: 203-432-6144. E-mail: gary.brudvig@yale.edu.

Notes

The authors declare no competing financial interest.

ACKNOWLEDGMENTS

We thank Clyde Cady for help with the diffuse reflectance UV/visible spectroscopic experiments, Ping-Yu Chen for help with the EPR experiments, Gözde Ulas for advice on the O_2 assay, the Yale Richards Center for allowing us to use the supercomputer to do DFT calculations, and James Blakemore for useful discussions. This work was supported by the Chemical Sciences, Geosciences, and Biosciences Division, Office of Basic Energy Sciences, Office of Science, U.S. Department of Energy (DE-FG02-07ER15909).

REFERENCES

(1) McEvoy, J. P.; Brudvig, G. W. *Chem. Rev.* **2006**, *106*, 4455.
(2) Yachandra, V. K.; Sauer, K.; Klein, M. P. *Chem. Rev.* **1996**, *96*, 2927.
(3) Peloquin, J. M.; Campbell, K. A.; Randall, D. W.; Evanchik, M. A.; Pecoraro, V. L.; Armstrong, W. H.; Britt, R. D. *J. Am. Chem. Soc.* **2000**, *122*, 10926.
(4) Britt, R. D.; Peloquin, J. M.; Campbell, K. A. *Annu. Rev. Biophys. Biomolec. Struct.* **2000**, *29*, 463.
(5) Umena, Y.; Kawakami, K.; Shen, J.-R.; Kamiya, N. *Nature* **2011**, *473*, 55.

(6) Cady, C. W.; Crabtree, R. H.; Brudvig, G. W. *Coord. Chem. Rev.* **2008**, *252*, 444.
(7) Mukhopadhyay, S.; Mandal, S. K.; Bhaduri, S.; Armstrong, W. H. *Chem. Rev.* **2004**, *104*, 3981.
(8) Wang, S. Y.; Huffman, J. C.; Folting, K.; Streib, W. E.; Lobkovsky, E. B.; Christou, G. *Angew. Chem., Int. Ed. Engl.* **1991**, *30*, 1672.
(9) Wemple, M. W.; Tsai, H. L.; Wang, S. Y.; Claude, J. P.; Streib, W. E.; Huffman, J. C.; Hendrickson, D. N.; Christou, G. *Inorg. Chem.* **1996**, *35*, 6437.
(10) (a) Vincent, J. B.; Christmas, C.; Huffman, J. C.; Christou, G.; Chang, H. R.; Hendrickson, D. N. *J. Chem. Soc., Chem. Commun.* **1987**, 236. (b) Vincent, J. B.; Christmas, C.; Chang, H. R.; Li, Q. Y.; Boyd, P. D. W.; Huffman, J. C.; Hendrickson, D. N.; Christou, G. *J. Am. Chem. Soc.* **1989**, *111*, 2086.
(11) Kulawiec, R. J.; Crabtree, R. H.; Brudvig, G. W.; Gayle, K.; Schulte, G. K. *Inorg. Chem.* **1988**, *27*, 1309.
(12) Vincent, J. B.; Chang, H. R.; Folting, K.; Huffman, J. C.; Christou, G.; Hendrickson, D. N. *J. Am. Chem. Soc.* **1987**, *109*, 5703.
(13) Chan, M. K.; Armstrong, W. H. *J. Am. Chem. Soc.* **1991**, *113*, 5055.
(14) Dube, C. E.; Wright, D. W.; Pal, S.; Bonitatebus, P. J.; Armstrong, W. H. *J. Am. Chem. Soc.* **1998**, *120*, 3704.
(15) Wieghardt, K.; Bossek, U.; Nuber, B.; Weiss, J.; Bonvoisin, J.; Corbella, M.; Vitols, S. E.; Girerd, J. J. *J. Am. Chem. Soc.* **1988**, *110*, 7398.
(16) Hagen, K. S.; Westmoreland, T. D.; Scott, M. J.; Armstrong, W. H. *J. Am. Chem. Soc.* **1989**, *111*, 1907.
(17) Wang, S.; Tsai, H. L.; Streib, W. E.; Christou, G.; Hendrickson, D. N. *J. Chem. Soc., Chem. Commun.* **1992**, 1427.
(18) Wang, S. Y.; Tsai, H. L.; Hagen, K. S.; Hendrickson, D. N.; Christou, G. *J. Am. Chem. Soc.* **1994**, *116*, 8376.
(19) Ruettinger, W. F.; Campana, C.; Dismukes, G. C. *J. Am. Chem. Soc.* **1997**, *119*, 6670.
(20) Gedye, C.; Harding, C.; McKee, V.; Nelson, J.; Patterson, J. *J. Chem. Soc., Chem. Commun.* **1992**, 392.
(21) Wang, S. Y.; Folting, K.; Streib, W. E.; Schmitt, E. A.; McCusker, J. K.; Hendrickson, D. N.; Christou, G. *Angew. Chem., Int. Ed. Engl.* **1991**, *30*, 305.
(22) Bashkin, J. S.; Chang, H. R.; Streib, W. E.; Huffman, J. C.; Hendrickson, D. N.; Christou, G. *J. Am. Chem. Soc.* **1987**, *109*, 6502.
(23) Mukhopadhyay, S.; Staples, R. J.; Armstrong, W. H. *J. Chem. Soc., Chem. Commun.* **2002**, 864.
(24) Philouze, C.; Blondin, G.; Girerd, J. J.; Guilhem, J.; Pascard, C.; Lexa, D. *J. Am. Chem. Soc.* **1994**, *116*, 8557.
(25) Philouze, C.; Blondin, G.; Menage, S.; Auger, N.; Girerd, J. J.; Vigner, D.; Lance, M.; Nierlich, M. *Angew. Chem., Int. Ed. Engl.* **1992**, *31*, 1629.
(26) Chen, H. Y.; Faller, J. W.; Crabtree, R. H.; Brudvig, G. W. *J. Am. Chem. Soc.* **2004**, *126*, 7345.
(27) Chen, H.; Collomb, M.-N.; Duboc, C.; Blondin, G.; Riviere, E.; Faller, J. W.; Crabtree, R. H.; Brudvig, G. W. *Inorg. Chem.* **2005**, *44*, 9567.
(28) Suzuki, M.; Hayashi, Y.; Munezawa, K.; Suenaga, M.; Senda, H.; Uehara, A. *Chem. Lett.* **1991**, 1929.
(29) Brimblecombe, R.; Swiegers, G. F.; Dismukes, G. C.; Spiccia, S. *Angew. Chem., Int. Ed.* **2008**, *120*, 7445.
(30) Hocking, R. K.; Brimblecombe, R.; Chang, L.-Y.; Singh, A.; Cheah, M. H.; Glover, C.; Casey, W. H.; Spiccia, L. *Nature Chem.* **2011**, *3*, 461.
(31) Limburg, J.; Vrettos, J. S.; Liable-Sands, L. M.; Rheingold, A. L.; Crabtree, R. H.; Brudvig, G. W. *Science* **1999**, *283*, 1524.
(32) Limburg, J.; Vrettos, J. S.; Chen, H. Y.; de Paula, J. C.; Crabtree, R. H.; Brudvig, G. W. *J. Am. Chem. Soc.* **2001**, *123*, 423.
(33) Yagi, M.; Narita, K. *J. Am. Chem. Soc.* **2004**, *126*, 8084.
(34) Narita, K.; Kuwabara, T.; Sone, K.; Shimizu, K.; Yagi, M. *J. Phys. Chem. B* **2006**, *110*, 23107.
(35) Baffert, C.; Romain, S.; Richardot, A.; Leprêtre, J.; Lefebvre, B.; Deronzier, A.; Collomb, M. *J. Am. Chem. Soc.* **2005**, *127*, 13694.
(36) Frisch, M. J.; Trucks, G. W.; Schlegel, H. B.; Scuseria, G. E.; Robb, M. A.; Cheeseman, J. R.; Montgomery, J. A., Jr.; Vreven, T.; Kudin, K. N.; Burant, J. C.; Millam, J. M.; Iyengar, S. S.; Tomasi, J.; Barone, V.; Mennucci, B.; Cossi, M.; Scalmani, G.; Rega, N.; Petersson, G. A.; Nakatsuji, H.; Hada, M.; Ehara, M.; Toyota, K.; Fukuda, R.; Hasegawa, J.; Ishida, M.; Nakajima, T.; Honda, Y.; Kitao, O.; Nakai, H.; Klene, M.; Li, X.; Knox, J. E.; Hratchian, H. P.; Cross, J. B.; Bakken, V.; Adamo, C.; Jaramillo, J.; Gomperts, R.; Stratmann, R. E.; Yazyev, O.; Austin, A. J.; Cammi, R.; Pomelli, C.; Ochterski, J. W.; Ayala, P. Y.; Morokuma, K.; Voth, G. A.; Salvador, P.; Dannenberg, J. J.; Zakrzewski, V. G.; Dapprich, S.; Daniels, A. D.; Strain, M. C.; Farkas, O.; Malick, D. K.; Rabuck, A. D.; Raghavachari, K.; Foresman, J. B.; Ortiz, J. V.; Cui, Q.; Baboul, A. G.; Clifford, S.; Cioslowski, J.; Stefanov, B. B.; Liu, G.; Liashenko, A.; Piskorz, P.; Komaromi, I.; Martin, R. L.; Fox, D. J.; Keith, T.; Al-Laham, M. A.; Peng, C. Y.; Nanayakkara, A.; Challacombe, M.; Gill, P. M. W.; Johnson, B.; Chen, W.; Wong, M. W;. Gonzalez, C.; Pople, J. A. *Gaussian 03, revision D.01*; Gaussian, Inc., Wallingford, CT, 2004.
(37) Manivel, A.; Ilayaraja, N.; Noel, V. M. *Electrochim. Acta* **2007**, *52*, 7841.
(38) Morrison, M. M.; Sawyer, D. T. *Inorg. Chem.* **1978**, *17*, 333.
(39) Tyryshkin, A. M.; Watt, R. K.; Baranov, S. V.; Dasgupta, J.; Hendrich, M. P.; Dismukes, G. C. *Biochemistry* **2006**, *45*, 12876.
(40) Klewicki, J. K.; Morgan, J. J. *Environ. Sci. Technol.* **1998**, *32*, 2916.
(41) Wang, Y.; Zhu, J.; Han, J.; Guo, R. *Nanotechnology* **2008**, *19*, 405606.
(42) Tagore, R.; Chen, H.; Zhang, H.; Crabtree, R. H.; Brudvig, G. W. *Inorg. Chim. Acta* **2007**, *360*, 2983.
(43) Sproviero, E. M; Gascón, J. A.; McEvoy, J. P.; Brudvig, G. W; Batista, V. S. *J. Am. Chem. Soc.* **2008**, *130*, 3428.
(44) Hull, J. F.; Balcells, D.; Blakemore, J. D.; Incarvito, C. D.; Eisenstein, O.; Brudvig, G. W.; Crabtree, R. H. *J. Am. Chem. Soc.* **2009**, *131*, 8730.